RESEARCH ARTICLE



Dissolved organic matter from surface and pore waters of a discontinuous permafrost watershed in central Alaska reveals both compositional and seasonal heterogeneity

Kristin R. Gagné¹ · Bridget A. Eckhardt² · Katey M. Walter Anthony² · David L. Barnes² · Jennifer J. Guerard³

Received: 15 July 2022 / Accepted: 16 December 2022

This is a U.S. Government work and not under copyright protection in the US; foreign copyright protection may apply 2023

Abstract

In areas of active permafrost thaw, changes in organic carbon pools may significantly impact water quality and ecosystem services across the landscape. Surface and pore waters were collected from streams and lakes in the Goldstream Valley near Fairbanks Alaska over a period of three years, 2016–2018, to compare and contrast different thermokarst regimes, their water quality, and dissolved organic matter (DOM). Waters were characterized by elemental analysis, major ions, and optical characterization of DOM. We found DOM composition to be spatiotemporally heterogeneous, and influenced by complex hydrology. This result is evidenced by analyzing DOM character between differing water bodies and depths, seasonality, as well extent of metal association with DOM. Pore water DOM overall varied from the surface waters, with respect to both optical metrics and seasonality. Optical parameters typically associated with terrestrial signals were observed to become more prevalent in pore waters as summer progressed toward winter in an active thermokarst lake, potentially corroborating a hypothesis of downward flow into the talik or rapid turnover of authochthonous-sourced DOM. In addition, winter sampling, where surface inputs were assumed to be frozen, is essential to observe annual patterns of DOM composition. A principal components analysis separated water bodies based on their thermokarst activity and by season. Dissolved organic matter in these permafrost-impacted systems was found to be more complex than simply terrestrial or microbial, and extracted isolates from these waters were not necessarily bounded by existing end-member references.

Keywords Humic substances · Dissolved organic matter · Permafrost · Thermokarst · Aquatic geochemistry

Introduction

Northern permafrost soils hold the largest pool of terrestrial organic matter, estimated at 1307 Gt C (Schuur et al. 2015). A large portion (25–35%) of this carbon exists in yedoma, which consists of icy, organic-rich silt-dominated syngenetic permafrost soils formed during the Pleistocene (Strauss et al. 2017). It has been substantially modified by warming and hydrology during the Holocene (Strauss et al.

☑ Jennifer J. Guerard guerard@usna.edu

Published online: 09 January 2023

2017). Given their high ice content, yedoma permafrost soils are especially susceptible to abrupt thaw and talik development beneath thermokarst lakes (Walter Anthony et al. 2018; Strauss et al. 2017; Heslop et al. 2019; Schirrmeister et al. 2011; Olefeldt et al. 2016). When ice-rich permafrost thaws, ground surface collapse can lead to depressions that fill with water. This process can lead to substantial export of carbon and trace elements into the watershed (Kokelj et al. 2013; Kessler et al. 2012; Larouche et al. 2015). Thermokarst lakes have been estimated to cover 1.3×10^6 km² (Olefeldt et al. 2016) and this is likely to increase as more thermokarst lakes are formed in the future (Chin et al. 2016; Frey and McClelland 2009; Kokelj et al. 2013; Thienpont et al. 2013), releasing CH₄ and CO₂ (Elder et al. 2019; Walter Anthony et al. 2018; Winkel et al. 2019; and others). When thermokarst lakes drain, sediments may refreeze, forming less ice-rich soils that differ from their original late Pleistocene composition (Strauss et al. 2013; Walter Anthony et al. 2014).



Department of Chemistry and Biochemistry, University of Alaska Fairbanks, Fairbanks, AK 99775, USA

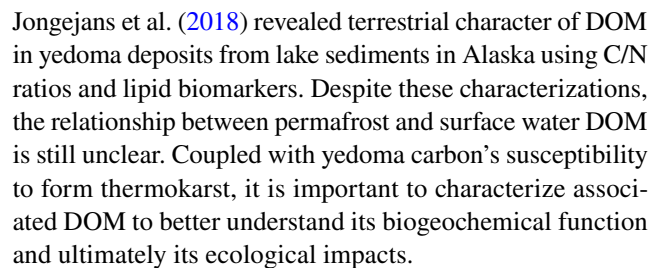
Water and Environmental Research Center, University of Alaska Fairbanks, Fairbanks, AK 99775, USA

³ Chemistry Department, United States Naval Academy, Annapolis, MD 21402, USA

Thermokarst features have the potential to remain active for long-periods of time at the edge of lakes, on the order of centuries to millennia, allowing them to help drive delivery of permafrost organic matter to surface waters (Abbott et al. 2014). Thawing permafrost is expected to release organic carbon, ions, and nutrients, which has been observed in the Yukon River Basin (O'Donnell et al. 2010; Toohey et al. 2016) and other permafrost-impacted sites (Kokelj et al. 2013; Kurek et al. 2022). Indeed, some studies (e.g., Kurek et al. 2022; Johnston et al. 2019) observed increases in dissolved organic carbon (DOC) concentration from spring through fall and into winter, along with shifts in optical properties as well, but to date, these studies are relatively few. Yedoma carbon represents some of the more characterized permafrost due to its high carbon content and potential biolability upon thaw (Neff et al. 2006; Vonk et al. 2013; Ewing et al. 2015; Spencer et al. 2015; O'Donnell et al. 2016; MacDonald et al 2021; Rogers et al. 2021), however seasonal influences on its contribution to surface waters are still relatively lacking, especially in winter. Understanding compositional shifts in dissolved organic matter (DOM) pools in permafrost-impacted systems across an entire annual cycle may help to elucidate contributions of permafrost to surface waters, its mobilization and mineralization. In addition, winter may be a lens through which to observe permafrost influences because active layer hydrology is limited due to the ground surface being frozen.

Water flowing through surface organic-rich soil layers increases DOC concentration (Frey and McClelland 2009), but determining the hydrology of such systems can be complex. Geochemical analyses are a powerful tool through which to understand changes in hydrology and water systems, framing the context around which DOM pools may be changing. Ions that complex or associate with organic matter may help to resolve carbon composition within certain water bodies. For example, Ba:Cl ratios have been shown to correlate with permafrost degradation in the Arctic during late thaw (Barker et al. 2014), while certain metal(loid)s may associate directly with DOM in ways dependent upon the composition of humic substances. The complexation of Fe and Al to DOM and their dependence upon composition has been observed in Arctic and sub-Arctic surface waters (Pokrovsky et al. 2018; Pokrovsky and Schott 2002; Stolpe et al. 2013; Weyhenmeyer et al. 2014). Other elements such as Sr may also adsorb favorably to proteinaceous components of organic matter (Boyer et al. 2018). Thus, altered DOM pools may influence geochemical parameters in the water column as well.

As permafrost organic carbon is typically "fresher" and less processed, with lower molecular weights and aromaticity, it may have especially biolabile groups such as reduced and saturated organics (Heslop et al. 2019; Vonk et al. 2015; Knobloch et al. 2018; Drake et al. 2015). However,



This study characterized the seasonal DOM and geochemical composition of waters from three water bodies with active thermokarst, two without, and two streams within the Goldstream Creek Watershed, which is underlain by discontinuous yedoma permafrost in interior Alaska. Our objective was to fingerprint DOM compositional character from bulk optical and geochemical parameters to determine the influence of permafrost thaw and associated hydrology on the composition of humic substances within the DOM carbon pool. Based on our previous investigation showing that the composition and reactivity of DOM isolates vary in this watershed (Gagné et al. 2020), this study hypothesized that the composition of the whole (non-isolated) DOM pool in systems with active thermokarst would differ from those in systems without active thermokarst, by analyzing the optical properties of the DOM and linking it to the geochemistry of the studied waters. The permafrost contribution to DOM in lake water, sediment pore waters and streams is thus expected to increase in winter when surface active layers are largely frozen. To answer these hypotheses, the heterogeneity and seasonality of dissolved organic matter was characterized in thermokarst-lake environments containing original undisturbed yedoma, thawed yedoma in thermokarst-lake taliks, and refrozen thermokarst-lake sediments (Emond et al. 2018). We sampled the described surface waters year-round over a period of three years (June 2016–October 2018). In addition, pore waters were sampled coincidently from two of those lakes over the period of one year (June 2016-March 2017). Elemental and ion concentrations, as well as optical properties of the DOM pool were measured to ascertain impacts of seasonality and permafrost contributions. Aquatic samples were analyzed and compared against optical properties of extracted and IHSS isolates to place permafrost-impacted DOM in the context of existing end-members.

Methodology

Site description

Goldstream Valley is a small residential watershed (East Goldstream Creek sub-watershed) within the Tanana River watershed. The Goldstream Valley is located in sub-Arctic Fairbanks, Alaska (Emond et al. 2018). It is underlain by



discontinuous permafrost with a mean annual air temperature of – 2.4 °C with a mean annual precipitation of 274 mm (Fairbanks Int. Airport, 1981–2010, U.S. National Climatic Data Center) and has been described previous (Gagné et al. 2020). The watershed is covered by boreal forest vegetation of black spruce (*Picea mariana*), white spruce (*Picea glauca*), moss (*Hylocomium spp.*), alder (*Alnus viridis*), and tussock cotton grass (*Eriophorum vaginatum*), with no previous glacier coverage. The thermokarst lakes and streams overlay Pleistocene yedoma permafrost (Table 1), which is rich in organic carbon and ice (Elder et al. 2019). These water bodies are situated in a complex quaternary deposit formed by silt and gravel deposition (Elder et al. 2019; Muhs and Budahn 2006).

In total, three lakes, two ponds, and two streams were sampled over the study period of June 2016-October 2018 (Table 1, Fig. 1). The characterization of the hydrology of the water bodies in this system is complicated by discontinuous permafrost, due to the potential of different flow paths (macropores, inter-hummock regions, and water tracks) (Carey and Woo 2000; O'Donnell and Jones 2006), and that lateral flow into lakes may still be possible through shallow aguifers or surface water runoff (Olid et al. 2022). In addition, streams in this watershed meander through areas of various talik formation extent, and thus may have varied contributions from thaw. Goldstream Creek was sampled in two locations. The first site (GSC1) is primarily upstream of most of the sampled lake/pond sites as well as residential areas, and the second site (GSC2) is further downstream of the sampled lake/pond sites. O'Connor Creek (OCC) comes from the north before it ultimately connects with Goldstream Creek.

The central part of Goldstream Lake (GSL) has been dated to around 1000 years old, though the thermokarst margin is under 60 years old, and most likely a closed talik (Walter Anthony et al. 2021). Blacksheep Pond (BSP) is a second-generation lake formed in the refrozen lake sediments of former drained basins, less than 60 years old and also a closed talik (Walter Anthony et al. 2021). Doughnut Lake (DNL) is considered to be an open talik, with stable margins. Octopus Lake (OCT) is over 1000 years old, however its northern and southern basins joined via thermokarst sometime after 1949, after which shorelines have remained stable (Walter Anthony, unpublished data). O'Brien Pond (OBP) is the remnant of a thawed pingo, and likely formed when the adjacent road was made. A pingo can form when groundwater recharges in areas without permafrost up-gradient of the watershed and becomes trapped and under pressure in lower areas beneath permafrost. Such artesian conditions are commonly observed in watersheds underlain with ice-rich permafrost, as the permafrost forms an impenetrable barrier separating the supra-permafrost and sub-permafrost portions of the aquifer (Callegary et al. 2013; Yoshikawa and Hinzman 2003).

Sample collection

Samples were collected from over a period between March 2016 and October 2018 near bimonthly during spring thaw, summer, fall freeze up, and winter seasons (see Tables S1–S3 for n values during each season, and Figs S1, S2 for frequency of sampling each site). Samples were taken from both surface and bottom depths, with the exception of BSP and OBP which were too shallow to develop a thermocline.

Table 1 Study site and sampling characteristics

Name	Abbr	Lat. (°N)	Long. (°W)	Surface Area (m ²)	Max depth (m)	Active thermokarst?	Sampled depths (cm)
Goldstream L.	GSL	64.916	- 147.848	10,000	4.7	Yes	10 and ~ 300
Pole E	GSLPE						-90.6 to -292.6
Pole C	GSLPC						-90.5 to -290.6
Doughnut L.	DNL	64.899	- 147.908	34,000	3.8	No	10 and ~ 200
Pole E	DNLPE						-170.6 to -370.6
Pole C	DNLPC						-296.3 to -497.9
Octopus L.	OCT	64.907	-147.860	22,000	2	No	10 and ~ 200
O'Brien P.	OBP	64.910	- 147.914	530	<2	Thawed Pingo	10
Blacksheep P.	BSP	64.888	- 147.920	540	<2	Yes	10
Goldstream Cr.	GSC1	64.912	- 147.832	_	_	_	10
	GSC2	64.909	- 147.948	_	_	_	10
O'Connor Cr.	OCC	64.915	- 147.899	_	_	_	10

All lakes formed in yedoma-type permafrost soils, but during the 2016–2018 study period were subject to varying degrees of thermokarst activity. GSL, DNL, and OCT were sampled at two depths—10 cm for epilimnion, and just above bottom at sampling location for hypolimnion. In addition, GSL and DNL each had two pore-water sampling locations installed via drive poles (PE, PC): Pole E near the eastern margin of the lake, and Pole C near the center of the lake



31 Page 4 of 16 K. R. Gagné et al.

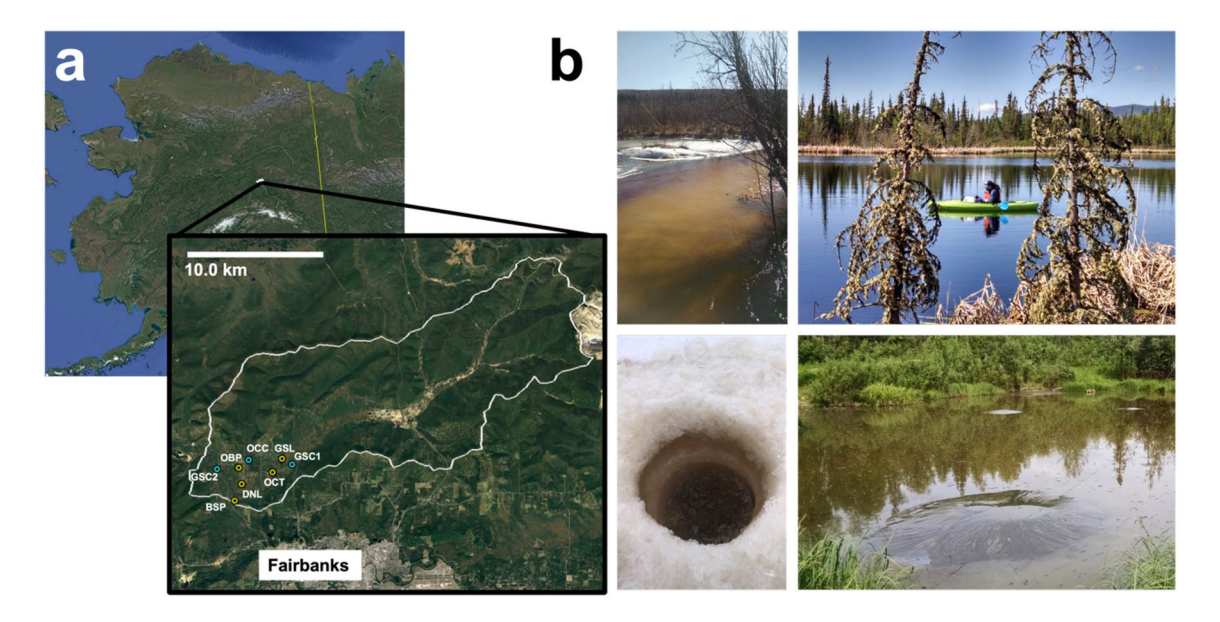


Fig. 1 a Map of Sampling locations withing Goldstream Watershed. Blue: streams; Yellow: lakes and ponds. **b** Selected sampling images. From top left, clockwise: Goldstream Cr. (*GSC2*), April 2016. Goldstream Cr. (*GSC2*), April 2016.

stream L. (*GSL*), June 2017. O'Brien P. (*OBP*), June 2016. Octopus L. (*OCT*), March 2016 (Color figure online)

Streams were not as frequently sampled due to thick ice pack during winter months and safety concerns during freeze and thaw water sampling.

At the time of collection, a YSI hydrolab probe was utilized during sampling days where warmer temperatures allowed for probe usage (> -10 °C) and the following was obtained: pH, temperature, dissolved oxygen, and conductivity. Surface samples (~10 cm depth) were collected in 250 mL brown acid-washed polyethylene bottles and placed in a cooler until transported to the laboratory. Bottom water samples were collected using a Van Dorn sampler sent to the bottom of the lake and rinsed before collection. Upon return to the laboratory, samples were filtered using 0.45 µm polypropylene filters and run immediately for absorbance and fluorescence, or samples were acidified with HCl in muffled glass vials for DOC quantification, or diluted to 2% omnitrace HNO3 in acid-washed brown HDPE bottles for ICP-MS and stored in the dark at 4 °C, or transferred to HDPE bottles and placed into a − 18 °C freezer for ion chromatography (IC).

Sampling poles were installed at two locations within Goldstream Lake and Doughnut Lake. Pole 1 (PE; Pole Edge) was installed on the eastern edge of the lake where thermokarst of GSL is actively expanding (Water Anthony et al. 2018), and Pole 2 (PC; Pole Center) in the center. The poles were installed during the winter to take advantage of stable ice cover platform. Each is driven to a different depth within the sediment ranging from 3 to 4.5 m, and outfitted with five rhizon soil solution samplers (RSSS) to obtain water samples from within the sediments using a process

similar to the methodology described by Alberto et al. (2000). The RSSS are comprised of 5-cm long porous polymer tubes with pore sizes of approximately 0.2 µm. Lake sediment water (in-situ pore water) samples were obtained by attaching acid-washed 60-mL syringes to the RSSS sampling points. A vacuum was applied to each sampling point and the syringes were held open with customized PVC pipe. Syringes were left to come to equilibrium over a period of 3 to 5 days before samples were collected. The amount of water collected from each syringe varied greatly (often less than 10 mL total). In some cases, not all samples could be collected and not from all depths, either due to small volumes obtained from the syringes, or in some of the winter samplings, the lines connecting the syringes to the RSSS froze, prohibiting acquisition of samples. In these cases, optical parameters and DOC quantification were prioritized over cations.

Instrumentation

A list of chemicals used is provided in the Supplementary Information. Absorbance and fluorescence were run on filtered water samples in a 1 cm quartz cuvette on an Aqualog–800–C (Horiba Instruments, Edison, NJ, USA). Absorbance was run from 200–800 nm every 1 nm with 0.1 s integration time. The ratio of slopes (S_R) between 275–295 nm and 300–350 nm was determined according to Helms et al. (2008). E2:E3 was determined following (Peuravuori and Pihlaja 1997) and SUVA₂₅₄, or specific ultraviolet absorbance at 254 nm, was computed using



absorbance at 254 nm normalized to DOC concentration (Weishaar et al. 2003). Fluorescence excitation emission matrices were run from 200-600 nm excitation every 3 nm, and 240-600 nm emission every 4 px (2.33 nm), with an integration time of 0.1 s. Samples were diluted to absorbance < 1.0 A. U. at 254 nm prior to fluorescence. Excitation emission matrices were blank subtracted, corrected for instrument correction factors, Rayleigh scattering removed, and inner filter correction applied according to Cory et al. (2010). Raman normalization and subsequent computation of fluorescence ratios: fluorescence index (FI, $\lambda_{ex} = 370$ nm; $\lambda_{\rm em} = 470/520$ nm, Cory et al. 2010), humification index (HIX, $\lambda_{\rm ex} = 254$ nm, $\lambda_{\rm em} =$ area from 435–480 nm/(total area 300-345 nm + 435-480 nm), Ohno 2002), and biological index (BIX, λ_{ex} = 310 nm; λ_{em} = 380/430 nm, Huguet et al. 2009) were determined with Matlab v.R2017a (Mathworks, Natick, MA, USA). Total iron concentrations (measured as described below) were used to correct SUVA₂₅₄ values according to methods in Poulin et al. (2014) and are previously described (Gagné et al. 2020).

All elemental and ion measurements utilized quality control samples and blank checks every 10-15 samples with external calibration curves. Metal(loid) concentrations in surface waters were determined using an Agilent 7500ce (Agilent Technologies, Santa Clara, CA, USA) inductively coupled plasma-mass spectrometer (ICP-MS) following EPA method 200.8 (US EPA 1994). Metal(loid)s specifically analyzed included the following, based on prevalence of detectable concentrations and biogeochemical relevance: Na, Mg, Al, K, Ca, Mn, Fe, As, Sr, Sb, and Ba. An internal standard of Ge, Y, Sc, Rh, and Ir was used, along with reference standards (SLRS-5 and NIST 1640a) to ensure proper tuning and quality assurance/control. Metals for pore waters were determined by microwave plasma (MP)-Atomic Emission Spectroscopy (AES) on an Agilent MP-AES 4200 for Na, Mg, K, and Ca, in samples preserved with 5% HNO₃ and filtered to 1.5 µm.

Select fresh water samples were analyzed for size fraction analysis of the DOM fraction using a Postnova AF2000-FFF (Postnova Analytics, Landsberf, Germany) coupled to a UV-Vis diode array detector (UV-DAD; Shimadzu SPD-M20A; Shimadzu Scientific Instruments, Columbia MD, USA) prior to ICP-MS analysis. Samples were simultaneously collected using a PostNova fraction collector in acid-washed metal free 13×100 mm polystyrene test tubes. The FFF channel was equipped with a 500 µm spacer and a 300 Da nominal cutoff polyethersulfone (PES) membrane using 5 mM ammonium acetate mobile phase, while the UV-DAD detector was set to a wavelength of 254 nm and 280 nm. Two separate injections were completed through injecting 400 µL 0.45 µm filtered samples onto the FFF membrane to get adequate sample amounts for fractions. Fractions were then collected during the duration of time NOM was observed through the UV-DAD at a minute a piece for each tube, all tubes that were observed in collecting through the UV-DAD detector were compiled and acidified to a 2% HNO₃ solution prior to analysis by ICP-MS.

Anion concentrations were quantified using either a Dionex ICS 5100 (Thermo Fisher Scientific, Waltham, MA, USA) equipped with an AG18 2 mm diameter guard column and AS18 2 mm diameter column, or a Dionex ICS 2000 equipped with Metpac, AG22 fast 2 mm diameter guard column, AS22 fast 2 mm diameter column, both with an eluent of 4.5 mM Na carbonate + 1.4 mM Na bicarbonate with an isocratic method at 0.30 ml min⁻¹. Chloride and sulfate were the only anions quantitatively observed, due to high carbonate concentrations obscuring the anion spectra. Total non-purgeable organic carbon and total dissolved nitrogen (TDN) were run on a Shimadzu TOC-L CPH (Shimadzu Scientific Instruments, Columbia MD, USA; LOQ = 0.1 mg CL^{-1} , LOQ = 0.05 mg NL^{-1}) using non-dispersive, infrared gas analysis following combustion organic carbon content of samples.

Statistical approach

Statistical analysis was conducted using Prism v.9.4.0 (GraphPad; San Diego, CA, USA). Two-way ANOVA was conducted to determine if measured concentrations varied between sampled waters or between seasons to a threshold of p < 0.05. Given that variances were found to be significantly different between most water bodies and seasons (Table S4), for specific differences between sample sets, unpaired t tests with welch's correction (no assumption of consistent standard deviations) were conducted, specifically: between seasons for specific samples, between water bodies, and depths (hypolimnion and epilimnion vs. pore waters) to a threshold of p value < 0.05.

Principal component analysis (PCA) was run utilizing z-score normalized parameters of slope ratio (S_R) , E2:E3, SUVA₂₅₄, DOC concentration, FI, HIX, BIX, and concentrations of major cations (Na, Mg, Al, K, Ca), as well as Fe. These were chosen because they were able to be obtained for most of the samples to be able to incorporate pore waters into the PCA model, and z-scores helped attenuate large fluctuations in certain parameters such as iron and sodium concentrations. In total 141 out of 237 total collected samples were included in the PCA. PCA was performed using variables which both maximized the chemical diversity and the number of samples, as only samples with measurements for all the input loadings are utilized in a PCA model. This constraint led to a choice of: S_R , E2:E3, DOC concentration, TDN, SUVA₂₅₄, FI, HIX, Na, Mg, K, Ca, which included 141 samples across water bodies, seasons, and depths in the generation of the PCA model. Chloride and trace metals were not included in the PCA so that pore-water samples



(of which many were not able to be analyzed for anions and trace metals) could be, and Fe was not included in the PCA due to the small number of pore waters which yielded enough volume for Fe measurements and thus would have limited the inclusion of porewaters into the model.

Results

Surface waters

Overall, three seasonal cycles were captured from sampling March 2016-October 2018, as observed through measured water temperatures and ice when sampling. Winter months also correlated with average daily temperatures for sampling days to be below 0 °C. Typically ice coverage began in October and ended in late March. Several parameters correlated with these seasonal cycles, such as pH and conductivity, which rose over the summer season and then fell again during the winter-spring. Studied lakes are generally shallow (<5 m), but showed physical differences between epilimnion and hypolimnion, as shown by water temperatures and dissolved oxygen concentrations at time of sampling (Fig. S1). pH was on average lower in winters with a wide range of variance across samples (Tables S1-S3). Increases in dissolved oxygen in nearly all surface waters were observed in later summer (August-September), consistent with fall turnover and mixing between epilimnion and hypolimnion (Fig S3).

DOC concentrations were generally high but ranged widely, with average concentrations between 12.29 and 100 mg C/L across surface waters for sampled lakes and streams. The highest DOC concentration for both the epilimnion and hypolimnion was observed in GSL, while the lowest concentrations were observed in the stream waters (Figs. 2, S1). Measured optical indices also spanned a large range of generally terrestrial character (generally high SUVA₂₅₄, lower S_R , moderate E2:E3, moderate FI for whole waters, etc.), whose differences were not easily resolvable between water bodies or seasons simply by time series (Figs. S1, S2). Despite having a lower DOC concentration than the other lakes, OCT had a higher SUVA₂₅₄ over most of the time sampled (Figs. 2, S1), however these values may be inflated due to the excessive iron concentrations (Poulin et al. 2014). However, sometimes Fe concentrations were so high, that when correcting for iron, corrected SUVA₂₅₄ values became artificially low (for example when Fe was > 1 mg/L, a corrected SUVA₂₅₄ could be as low as 0.14 L/mg C/m). In addition, using a correction like this, one would have to assume that all the iron in solution is Fe (III) as the samples were allowed to be oxic and at circumneutral pH during analysis, which may or may not be the case depending on how DOM moieties may have stabilized any complexation of Fe(II) species. Thus, values are reported, uncorrected, with the understanding that iron proportionally impacts SUVA and other absorbance metrics, especially when iron concentrations are high. Major ions Na, Mg, Ca, and also Sr to some extent experienced a rise

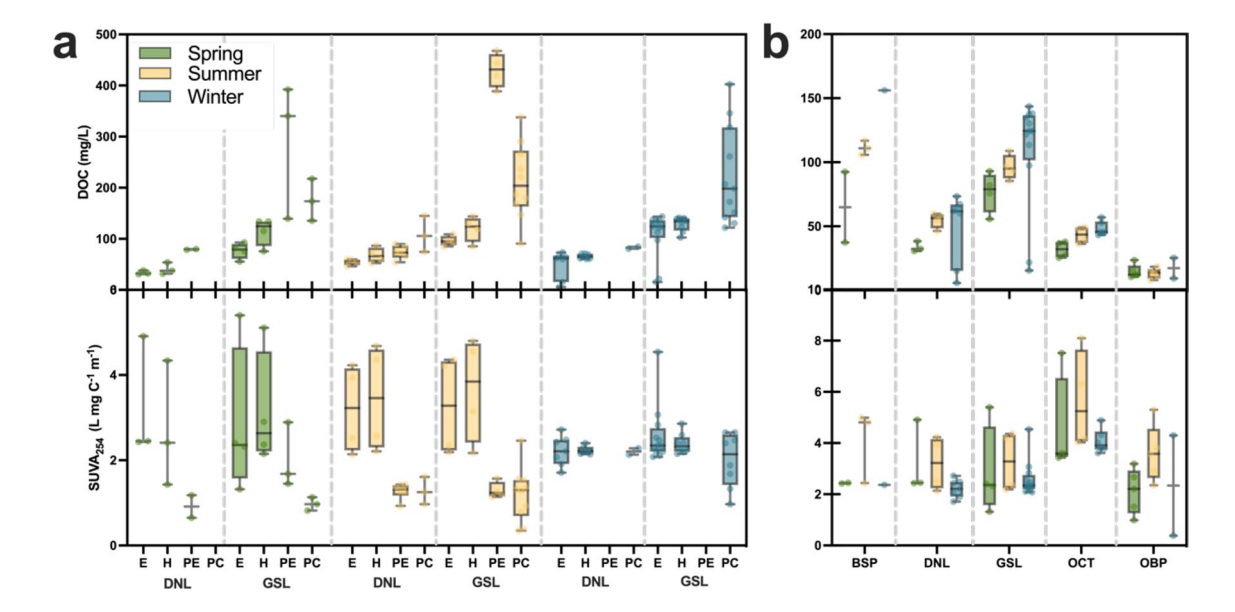


Fig. 2 DOC (top) and $SUVA_{254}$ (bottom) of differing lakes and sampled depths by season. **a** Doughnut L. (DNL) and Goldstream L. (GSL) at each depth: *E* epilimnion, *H* hypolimnion, *PE* pore-water drive pole at lake edge; *PC* pore-water drive pole at lake center,

separated by season: Spring=May-Jun, Summer=Jul-Sept, Winter=Oct-Apr. **b** Epilimnion (E) DOC (top) and SUVA₂₅₄ (bottom) data only for all lakes and ponds by season: *BSP* blacksheep P., *OCT* octopus L., *OBP* O'Brien P



in concentration over summer periods, and then a decrease over the winter months (Fig. S2).

DOC concentration in general was higher in GSL and BSP than in DNL or OCT. While two-way ANOVA found that parameters varied significantly between specific water bodies sampled or between seasons (Table S4), few statistical differences between specific sample set means were found to be significant by t test, mainly due to small sample sizes (*n* often \leq 6). For the lakes, where both epilimnion and hypolimnion waters were sampled, no DOC measurements were found to be statistically different, however there were significant differences between hypolimnion and porewaters in GSL (Spring p = 0.0007; Summer p = 0.0006). Differences between DOC concentration in lakes were only found to be significant in the summer and not other seasons (Table S5). No differences in DOC concentration were found between specific stream samples within any given season. However, despite the differences in DOC concentration between lakes in the summer, optical properties between lakes only showed statistically significant differences between select spring and winter samples. Optical properties such as SUVA₂₅₄, S_R, E2:E3, and BIX were statistically different between some of the lakes in winter, and fewer lakes in the spring (Table S5; Fig. S3). FI and HIX did not show any significant differences between lakes or sampled waters.

For metals, GSL epilimnion and hypolimnion showed differences in Na, Mg, K, Ca, Fe, Sr, and Ba (Fig. S4). Meanwhile, DNL only varied with As concentration, and OCT only with Al. For this reason, water column measurements were combined together for clustering purposes in the PCA modeling. Of particular note are the exceptionally high iron concentrations in some of the surface waters, given the relatively oxic and pH neutral conditions. Fe concentrations reached as high as 5.29 mg L⁻¹ in surface waters (GSL) and 9.38 mg L⁻¹ (OCT) in bottom waters. Anion concentrations varied greatly, though showed few differences between epilimnion and hypolimnion waters (Fig. S2), with few apparent temporal trends.

Surface waters exhibited similar trends of increasing DOC concentration from spring through to winter, though few means of DOC concentration were statistically different due to low sample size (Fig. 2, Table S5). SUVA₂₅₄ values tended to decrease going into winter. Consistent with the time series in Fig. S1, fluorescent optical properties such as FI and BIX did not show as strong of trends when grouped by season (Fig. S3). There were no statistical differences in fluorescent optical properties between surface or pore waters within lakes, nor when comparing against seasons.

Generally, streams had lower values and variability in measured concentrations of constituents than the lake waters, with concentrations typical for streams in this watershed and the greater Yukon River Basin (Mutschlecner et al. 2018). However, despite significant variance between surface

waters and between seasons by ANOVA, there was no statistical difference in mean DOC concentrations between surface waters, and few differences between optical parameters by season. Variance in $SUVA_{254}$ and S_R was smaller in the summer for stream samples, though TDN tended to increase in winter samples, with OCC having the highest mean TDN values of the three sampling points. A higher proportion of OCC's flow path from its head waters to the sampling point is underlain by permafrost (Emond et al. 2018), which may explain more nitrogen content if there are fresher materials.

Many metal(loid)s showed a similar pattern with seasonality as DOC concentration, even if not statistically significant due to the low sample size, especially the +1 and +2 cations (Na, Mg, K, Ca, Sr, Ba) and Sb (Fig. S4). Others, such as Fe and Al, which are more likely to be present as +3 ions or other oxidation states (e.g., Mn, As), did not show such trends. Certain values reflect the background geology such as arsenopyrites and carbonates in the area, while others are more reflective of surface inputs and runoff.

Pore waters

The sampled pore waters were analyzed by DOC concentration, TDN, optical parameters, and major cations (Fig. S5). The two lakes yielded rather different patterns in depth profiles for measured parameters, though in general there were too few acquired parameters from DNL pore waters to resolve any temporal changes. DOC concentration in the pore water was on average higher in GSL than in DNL (Table S2), which also appeared to have variance in concentration with time and depth, as well as between poles (Fig. S5, Table S5). For example, average summer edge and central pole porewaters had a DOC concentration of 73.58 and 108.41 mg/L respectively for DNL, but nearly twice that at 429.77, and 212.55 mg/L for edge and central pore waters in GSL (Table S3). In general, DOC concentration tended to increase with depth, and there is a shift toward higher DOC concentration as the summer season advanced in the GSL poles (Fig. S5). Despite differences in DOC concentrations, optical parameters of the pore waters showed less variation between poles within a lake, or between lakes, indicating that while the content of the organic carbon was different, the compositional signatures may be less distinguishable. SUVA₂₅₄ values generally decreased for PE, but increased for PC across the summer season, suggesting relatively less terrestrial signature in PE and more terrestrial signature for PC. This trend is consistent with E2:E3 and S_R , where E2:E3 also increases for PE (S_R largely invariant) but decreases for PC into the winter months. Fluorescence parameters were not necessarily consistent with absorbances, as FI and BIX went up for all poles during the season. However, fluorescence is merely a small sub-pool of the chromophoric DOM pool, and thus trends in fluorescence may not reflect overall



trends in the DOM. In general, pore waters displayed higher DOC concentration but lower SUVA₂₅₄ than their requisite surface waters in all seasons except winter, however the low sample number from each season resulted in few statistically resolved differences (Fig. 2).

Fewer data for aqueous metal concentrations are available in the pore-water samples than the surface waters due to the low sample volumes obtained (Table S3). Despite this, stark differences in major cation concentrations can be seen between DNL and GSL pore waters. However, statistical significance between pore-water sampling sites (PE vs. PC) or compared to surface waters are largely unresolvable with the number of samples. In general, GSL has higher concentration of ions compared to DNL, with no apparent trends in depth with the exception of 1) Mg, which decreases with depth in GSL PC, and 2) in the winter months, Na increases. On their own it is difficult to make conclusions primarily from the cation data alone.

Relationship between DOM and geochemical parameters

Linear regressions between DOC concentration and the various optical and inorganic measurements were performed to understand which ions might be associating with DOM, indicative of source waters, or correlated with surface runoff and/or lateral flow. DOC concentration was found to correlate to +1 and +2 cations: Na, Mg, K, Ca, Sr, and Ba as well as Sb and TDN (Figs. S6, S7). No such correlation was observed for the other metals, nor for any analyzed anions. When color coded by water body, patterns emerge in the element:DOC plots, which appear to cluster by water body due largely to differences in DOC concentration ranges (e.g., Figs. 3, S6). GSL and BSP have the highest

DOC concentrations and often also the highest metal(loid) concentrations for those that correlate to DOC concentration, followed by DNL and OCT, with streams and OBP having the lowest DOC concentrations. When streams and OBP are plotted on this correlation, they do not necessarily fall on the same linear trend as the lakes (e.g., Fig. 3). This lack of correlation could possibly be due to the extent of association of that element to DOC, DOM composition, or the nature of hydrological source inputs. Despite the lack of change in DOC concentration, streams do show increases in certain cations (Na, Mg Ca, K) in winter months compared to spring, which may be indicative of meltwater diluting runoff concentrations as has been observed in other streams at this latitude (Mutschlecner et al. 2018).

Iron does not correlate to DOC concentration ($R^2 = 0.06$; Fig. 3). As Fe can complex to DOM (e.g., Poulin et al. 2014; Ohno et al. 2008), to understand the extent of association with DOM, field-flow fractionation was performed to isolate DOM and quantify associated metal(loid)s in samples collected May 2018. Of the metal(loid)s studied, only Fe had substantial percentage association with the 300 Da cutoff, with percent Fe associated with the 300 Da fraction dropping below 12% when Fe total was over 1 mg L^{-1} . Mg, K, Mn, Sr, all had percent association around 1.0% of the total dissolved element. Na. Al, Ca, As, Sb, Ba were all below detection limit (BDL) for the 300 Da fraction and thus association with DOM was assumed to be negligible. Water bodies with the highest total dissolved Fe generally had the smallest Fe concentrations in the 300 Da fraction (Fig. 4A, B), supporting the lack of correlation of Fe to DOC concentration. However, there is also no correlation with the concentration of Fe in the 300 Da fraction and DOC concentration (Fig. 4C). In addition, normalizing the Fe in the 300 Da fraction to DOC concentration resulted in no

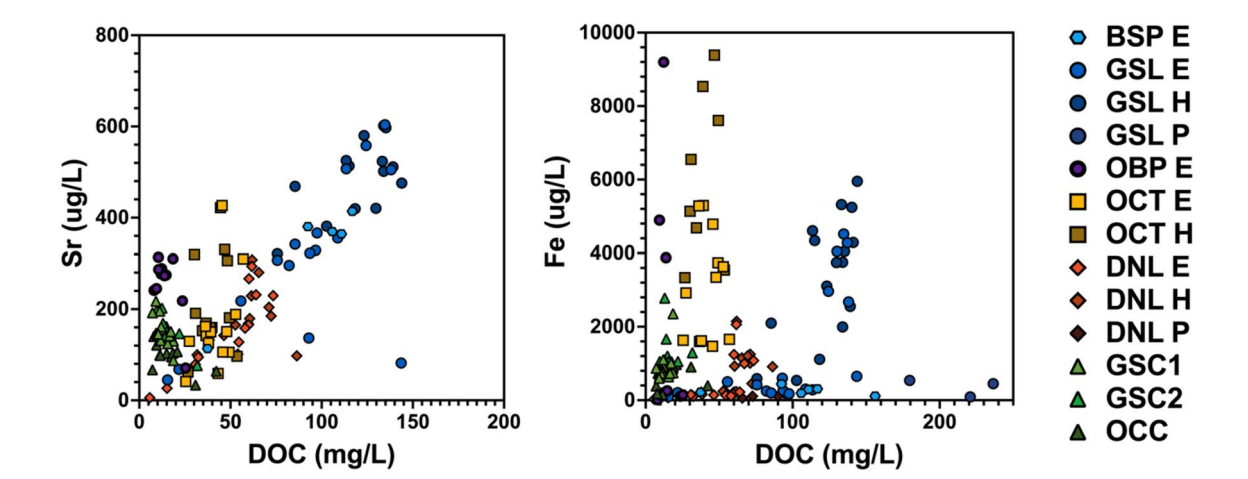


Fig. 3 Linear correlation of left: Sr and right: Fe by dissolved organic carbon (DOC) concentration. Orange colored data (diamonds, squares) represent open or transitional taliks. Blue colored data (cir-

cles) represent closed taliks. Green colored data (triangles) represent streams (Color figure online)



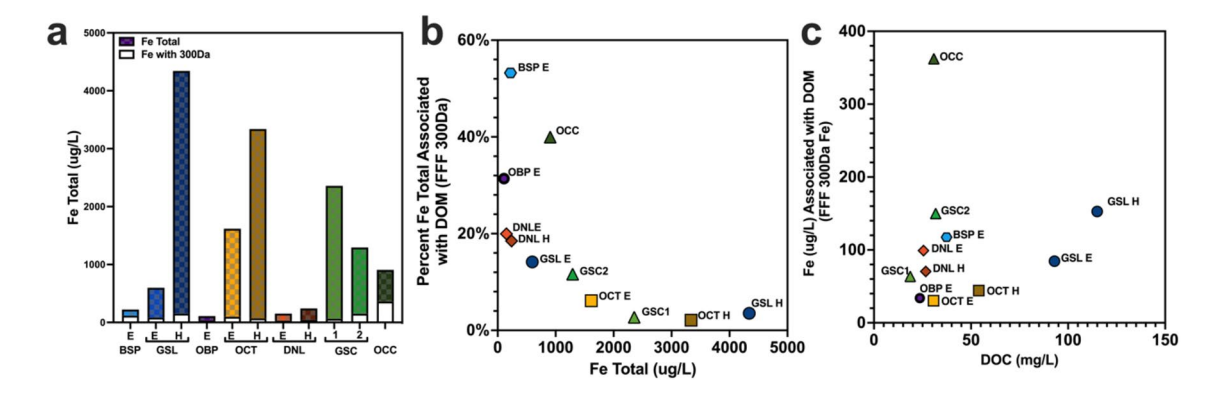


Fig. 4 Iron concentrations present in field-flow fractionation (FFF) 300 Da fraction. **a** Total Fe and 300 Da fraction for different water bodies. **b** Percent Fe associated with 300 Da fraction vs total Fe by

water body. c Total Fe associated with 300 Da fraction vs. DOC concentration (Color figure online)

correlation to optical properties with the exception of BIX $(R^2=0.5581, p=0.0207)$. However, as Fe can increase DOM absorbance or quench fluorescence (Ohno et al. 2008; Poulin et al. 2014; Stirchak and Donaldson 2021), this observation may simply be an artefact of the high total Fe. Even when SUVA₂₅₄ was corrected for Fe content (Poulin et al. 2014; Gagné et al. 2020), few correlations were observed.

Chloride does not correlate with parameters reflecting DOM composition and source (Fig. S8), and is likely to be reflective of surface runoff and lateral flow. Normalizing metal(loid) concentrations to chloride may yield information about which metal(loid)s are also possibly from runoff/lateral flow. Overall, relationships with selected metal(loid)s and chloride were weaker than that with DOC concentration. Relationships correlate most with + 1 and + 2 cations, as well as Sb (Fig. S8). However, when analyzing metal to chloride correlations by season, relationships such as with Ba which had been shown to be a marker of late fall inputs by permafrost in the Arctic (Barker et al. 2014) are not present in the current dataset.

Principal components 1 (PC1) and 2 (PC2) explained 40.11% and 12.25% of the total variance, respectively (Figs. 5, S9). As expected, SUVA₂₅₄'s loading is in the direction opposite of E2:E3 and FI, which trend to lower values being more terrestrial whereas SUVA₂₅₄ has higher values being terrestrial in character. It is interesting to note that DOC concentration and SUVA do not necessarily explain the same variance of the data set, as they are on opposite directions of PC1, which is consistent with the water body and seasonality comparisons between DOC concentration and SUVA₂₅₄ described above. Likewise, other elements that correlated well with DOC concentration appear in a similar location on the loadings plot as DOC concentration. Other optical parameters, such as S_R and HIX show more spread along PC2, and thus PC2 may be an indicator more of DOM compositional character. In the score plots (Fig. 5), scores are clustered by water body, with GSL and BSP on the negative axis of PC1, DNL and OBP around the origin of PC1 and slightly elevated in PC2, and then OCT and the streams on the most positive direction of PC1. Despite the clustering by water body, there was no separation of samples by depth in the PCA. When color coded by month, the winter samples within each water body appear the lower side of the cluster for that water body with respect to PC2.

Discussion

Thermokarst influence on DOM character

The observed higher DOC concentrations in water bodies with recent thermokarst activity is consistent with observations in other studies of permafrost-impacted systems (Frey and McClelland 2009; O'Donnell and Jones 2006; Prokushkin et al. 2007; Striegl et al. 2005, 2007). Increases in DOC concentration have been observed in permafrost-impacted streams of western Siberia (Frey and Smith 2005) and high Arctic thaw slumps (Grewer et al. 2016). In the PCA (Fig. 5) as well as several of the correlation plots (Figs. 3, S6), BSP and GSL, the two water bodies with active thermokarst, clustered together and also presented the highest DOC measurements, as high as 156.08 mg C/L. PC2 tracks negatively with HIX and to a lesser degree SUVA₂₅₄, but positively with S_R and to a small degree FI. Higher SUVA₂₅₄ and HIX values, and lower FI and S_R are often correlated with more terrestrial character or humification (Ohno 2002; Helms et al. 2008; Cory et al. 2010; Hansen et al. 2016). Thus, these optical parameters may indicate that GSL and BSP, despite their contact with a thaw margin, may actually overall have more terrestrial character of DOM, even if it was not necessarily resolved by t tests. This may be a result of surface contributions from active layer soils whose organic matter is highly



31 Page 10 of 16 K. R. Gagné et al.

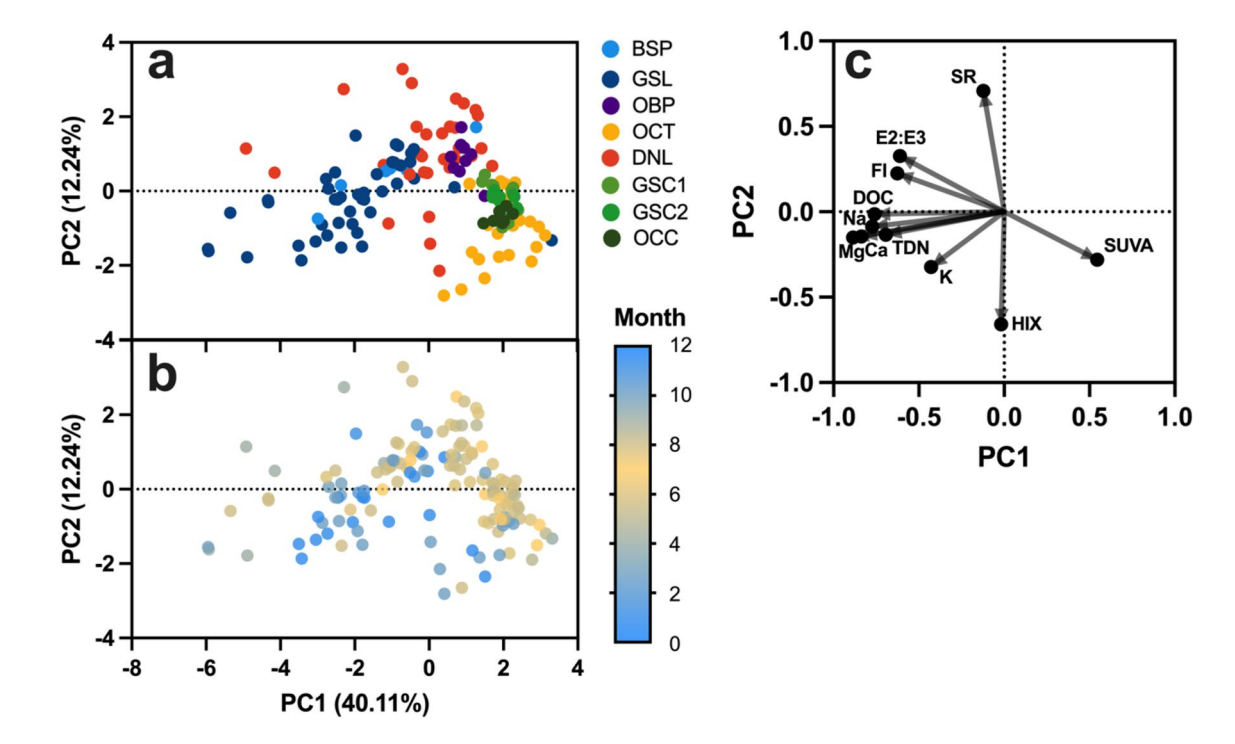


Fig. 5 PCA model of DOM and geochemical variables in the Goldstream Watershed. a Score plot of samples in the PCA, color coded by water body. Blue and purple colors indicate water bodies with active thermokarst, whereas yellow and orange colors indicate those without. Streams are colored green as they traverse areas of varied

permafrost coverage. b The same score plot of samples in the PCA, color coded by month of the year, with yellow centered around July for summer months and blue to represent winter months. c Loadings plot of the variables in the PCA model by component (Color figure online)

terrestrial in character (Gagné et al. 2020), or flow from lateral taliks (Eckhardt 2020), or perhaps merely a result of the vegetation accumulated at the bottom of the lake during its initial formation and subsidence. Of course, any of these optical parameters may be exaggerated by the presence of high iron, however, the exceptionally high total iron concentrations (> 1 mg/L) were detected in water bodies both with and without active thermokarst.

Aluminum and Fe are commonly known to associate with organic carbon (Pokrovsky and Schott 2002), however this study observed no correlation between DOC concentration and the two metals, in part to the very high concentrations in several water bodies. A positive correlation of Fe and DOC concentration has been previously observed in permafrostimpacted waters (Oleinikova et al. 2019; Pokrovsky and Schott 2002). The lack of positive correlation with Fe and DOC concentration in this study (Fig. 4) is likely instead caused by the large concentration of Fe saturating sites available for complexation with DOM (Weyhenmeyer et al. 2014). Metal(loid) to carbon relationships might not necessarily be explained by complexation, as field-flow fractionation results only showed Fe having significant complexation to the colloidal fraction of water samples. Mg, K, and Sr were the only other elements to have consistent detectable levels above the detection limits with the 300 Da fraction. This implies that the other inorganics quantified in this study are not associating with DOC, and any positive correlations observed may reflect another process, such as colocation within a source input rather than specific complexation.

With the exception of Al, Fe, and As, nearly all of the highest metal(loid) concentrations were detected in GSL and BSP. (Fig. S2), the water bodies with active thermokarst. In addition, for several of the measured concentrations, GSL pore waters exhibit higher concentrations than DNL pore waters (Fig. S5). Higher metal concentrations are consistent with other studies in permafrost-impacted systems, where major metals (Ca, Mg, K, and Na) in streams are associated with increased permafrost degradation in the Arctic (Keller et al. 2007; Stottlemyer 2001) and sub-Arctic regions (Petrone et al. 2006, 2007) of Alaska, as well as Canadian streams affected by retrogressive thaw slumps (Kokelj et al. 2013; Lafrenière and Lamoureux 2013). These may be indicative of increased groundwater contributions, as they are regarded as relatively conservative in these systems (Frey and McClelland 2009; Vonk et al. 2015; Toohey et al. 2016). OBP, which is suspected to have increased groundwater input due to artesian conditions, did not necessarily result in higher concentrations of dissolved major metals (Fig. S4). However, several elements are elevated with respect to the measured DOC compared to the other lakes (Mg, Ca, Mn,



Sr, Sb, Figs. 3, S6), despite having similar DOM optical character. This could be indicative of groundwater contribution to OBP that is distinct from DOM inputs, and thus the DOM in OBP may represent primarily active layer sources.

Streams sampled in this study clustered tightly together within the PCA, which could be due to the fact that the stream sample sites are all near the bottom of the watershed's hydrologic gradient, or reflective of similar surface sources upstream of the sampling points. The streams are predominantly underlain by permafrost (Emond et al. 2018), and thus it is likely that the hydrology of the watershed provides streams with similar water sources through surface flow, and limited influx from groundwater, consistent with lower cation concentrations observed in the streams compared to the lakes. In addition, historically there has been dredging and placer mining (LaPerriere and Reynolds 1997; Spence 1994) for gold (Brown et al. 1982), which also likely explains the correlation of Fe to As through arsenopyrites (FeAsS). Historical dredging and placer mining altered the flow path of GSC1 (Lesh and Ridgway 2007) and thus may have also altered the source inputs and extent of thaw.

Seasonality of DOM in permafrost systems

The surface waters all exhibit similar trends of increasing DOC concentration toward winter with many varying significantly by season (Table S4). We suspect increasing DOC is not merely a product of meltwater diluting concentrations in the spring and/or evaporation over the summer season, since the pore waters also displayed this seasonality, but instead reflecting a difference of sources. In addition, times series of DOC showed a steady increase in DOC concentration in the lakes across winter months (Fig. S1). For DNL and GSL, surface waters shifts in DOM optical character differed across seasons compared to their pore waters (Figs. 2, S3). Winter decreases in SUVA₂₅₄ for surface waters are likely more dramatic than shown due to coincident increased total Fe in winter, impacting absorbance (Poulin et al. 2014). A winter decrease in SUVA₂₅₄ in all lakes, not just those with active thermokarst, may suggest degradation of vegetationderived DOM to less aromatic materials (Shatilla and Carey 2019) rather than an introduction of freshly mobilized DOM from permafrost, consistent with downward or lateral flow from deepened active layers (Eckhardt 2020). It is possible that the active layer did not fully freeze in winter, potentially allowing shallow lateral flow throughout the winter, as may have been the case at least in part for winter of 2017–2018. Indeed, incomplete refreeze in winter has already been demonstrated from *in-situ* ground temperatures since 2018 for study sites in this watershed (Farquharson et al. 2022). Likewise, it might be expected that water from a pingo would be indicative of sub-permafrost groundwater contributions flowing vertically upward in artesian conditions, but as a *thawed* pingo from an open talik, flow is not necessarily constrained by impenetrable barriers from permafrost (Callegary et al. 2013; Yoshikawa and Hinzman 2003). An unfrozen active layer in winters may help to explain why nearly all lakes saw increases in element concentrations over winter, but those increases were most dramatic for the water bodies with active thermokarst.

Several metal(loid)s varied with season in the studied water bodies (Na, Al, Ca, Mn, Fe, As, Sr, Ba; Table S4). However, others such as K and Mg did not. Iron and Al were slightly higher in streams and lake surface waters in the spring, which may indicate mobilization of these otherwise insoluble elements via DOM during spring freshet (Bagard et al. 2011). Positive correlations between Na, Mg, Ca, Sr, and Ba with chloride may indicate the presence of lateral surface flow contributions into the lakes rather than from permafrost thaw. Chloride was observed to only show minor increases due to permafrost degradation in sub-Arctic Canada streams (Kokelj et al. 2013), and thus, correlations with chloride may instead indicate leaching of adjacent surface soils assisted by precipitation (Lockwood et al. 1995; McNamara et al. 1997). The Goldstream watershed is underlain by carbonate rich schist (Schirrmeister et al. 2016). Weathering of calcite and carbonate minerals from the active layer (Keller et al. 2007) may be responsible for leaching some of these cations into the surface waters. Barker et al. (2014) found a positive correlation of Ba and chloride occurs in Arctic streams during active layer thaw depth maxima, however, normalizing to chloride failed to reveal any seasonal trends in the current study. Chloride could be indicative of surface sources in this instance, including late season rain increasing surface runoff around sampling sites that may convolute a seasonal signal. Overall, winter revealed a different carbon pool compared to spring and summer seasons, potentially due to the isolation from surface sources. The differences were not uniform across water bodies with and without active thermokarst. As thaw progresses, especially with a lack of freezing of the active layer, one may expect winter seasons to reflect DOM pool composition of more mixed sources, such as in spring and summer, and a distinction in winter seasons may become more difficult to observe. Thus, the timing of this sampling presents a unique opportunity to isolate the impacts of thaw on DOM composition.

Multidimensional characterization of dissolved organic matter in permafrost systems

When PCA is run with optical parameters alone (absorbance and fluorescence indices, DOC concentration, and TDN), similar clustering of lakes and seasonality is present, however the separation is less distinct (Fig. S10) The inclusion of geochemical variables allowed for more distinction along both axes, rather than predominantly along just one



axis. In the PCA shown above (Fig. 5), PC2 largely seems to be explained by optical indices, whereas PC1 is more dominated by elemental concentrations, and to some extent SUVA₂₅₄, though SUVA₂₅₄ may reflect Fe concentrations. Separation along geochemical parameters may contribute to the ability to differentiate between deeper and shallow source DOM inputs, which may partly explain why winter samples are not just lower along PC2 indicating more terrestrial consistent signals, but also lower along PC1, reflective of the increased ions. It is interesting to note that optical loadings do not separate solely along a single axis. SUVA₂₅₄ is almost directly opposite from FI and E2:E3, which may indicate a spectrum of terrestrial to microbial consistent character. However, HIX and S_R are nearly perpendicular to the other optical loadings, suggesting there is more dimensionality to the DOM optical character than a simple explanation of terrestrial to microbial sourcing. An example of this is that the overall high terrestrial signal evidenced by the optical indices could be reflected by multiple terrestrial sources of DOM in the surface and/or pore waters. These could include surface run off or lateral flow through the active layer soil into the lakes and stream waters, or leaching of a vegetation layer (including black spruce) which would have been on the soil surface at the time of lake formation and which may be poorly decomposed in the more oxygen depleted lake sediment, or possibly groundwater flow in contact with freshly thawing permafrost. Thus, there may be different terrestrial-character DOM pools compared to the active layer sources, and may not necessarily be distinguished by solely comparing simple bulk properties such as the optical parameters used in this study. However, by combining the optical parameters with the other concentrations and metrics used in the PCA in this study, analysis starts to reveal more nuanced

compositional differences of the DOM pools than a limited terrestrial-microbial characterization would otherwise allow.

Such a need for a more nuanced characterization of DOM pools is especially relevant when characterizing PPL isolates extracted from these same waters (data reported in Gagné et al. 2020). Compared to the surface waters, optical parameters of PPL isolates shift, as expected (Fig. 6). In general SUVA $_{254}$ decreases, which may be a function of a lack of retention of Fe in the PPL extraction process. The absorbance and fluorescence ratios all decrease as well. And while PPL isolates do not capture exactly the same carbon pool as IHSS references captured by XAD8 (Li et al. 2017), it is interesting to note that in several cases, IHSS end-member references bound (SUVA $_{254}$, FI, BIX) and don't bound (S_R , E2:E3, HIX) optical parameters, further corroborating that a simple description of extent of terrestrial character is not sufficient to fully describe the source inputs of the DOM pools.

Conclusion

In areas of active permafrost thaw, changes in organic carbon pools can potentially have significant impacts on water quality and the ecosystem services that organic matter provides to the landscape. Overall, it was found that DOM composition in a yedoma discontinuous permafrost watershed was found to be heterogeneous both temporally and spatially, and impacted by complex hydrological patterns. This is especially evident through differences in seasonal trends between surface and pore waters, as well as the extent of metal complexation by DOM. For example, optical parameters typically associated with terrestrial signals were observed to become more prevalent in pore waters

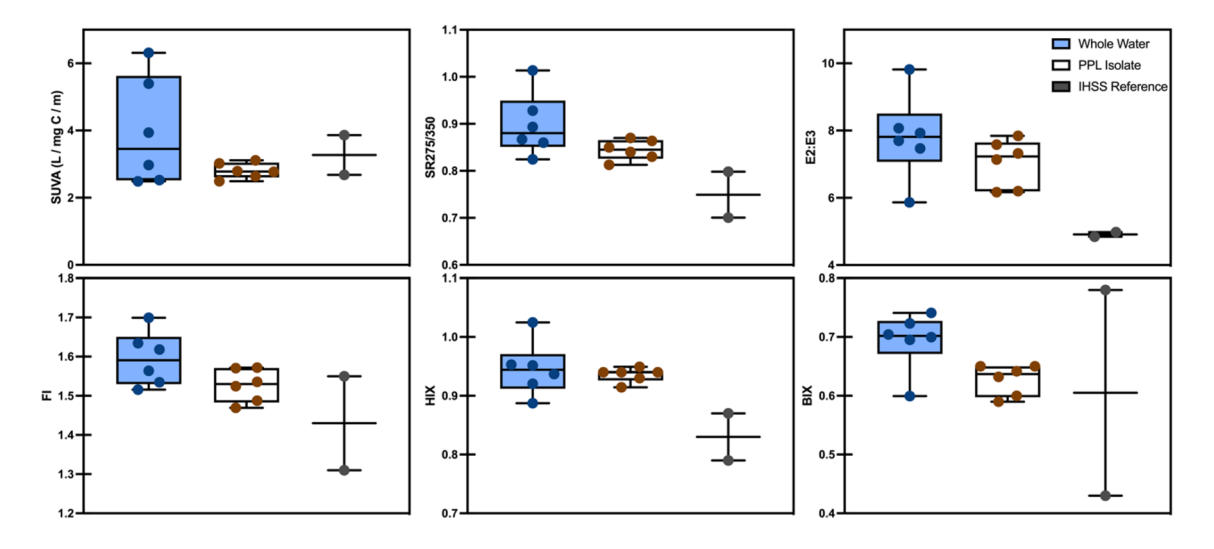


Fig. 6 Box and Whiskers plots of optical parameters for whole waters (blue) and corresponding PPL isolates (white) for BSP (Mar 2017), GSL (Jan 2017, Aug 2018), DNL (Jan 2017, Aug 2018), and OCT (Aug 2018), and IHSS reference isolates (PLFA, SRFA, black)



as summer progressed through winter in an actively thawing permafrost lake, potentially corroborating a hypothesis of downward flow into the talik. In addition, winter sampling, where surface inputs are frozen and thus negligible, is essential to observe annual cyclic patterns of organic matter composition and displayed shifts in not just geochemical parameters but also composition of that DOM. A principal components analysis distinguished water bodies by active thermokarst, as well as season of sampling. In doing so, optical properties of DOM in permafrost systems were revealed to be more complex than simply described as terrestrial or microbial, and PPL isolates from these waters were not necessarily bounded by existing endmember reference isolates. Together, the composition of DOM in permafrost-impacted waters is complicated by a number of hydrological, biogeochemical, and seasonal conditions, all of which together will influence the release, transformation, and ecological role of these substances in a changing climate.

Supplementary Information The online version contains supplementary material available at https://doi.org/10.1007/s00027-022-00930-y.

Acknowledgements This material is based in part upon work funded by NSF OPP-1500931, NASA through the Alaska Space Grant Program (80NSSC20M0070) Graduate Research Fellowship, and National Institutes for Water Resources Graduate Student-Led Proposal through the UAF Water & Environmental Research Center (WERC) and the USGS. Additional support to K. Walter Anthony came from NSF NNA 2022561.ICP-MS, and FFF were run at the UAF Advanced Instrumentation Laboratory (AIL). MP-AES and IC was run at the UAF WERC, and IC was also run at the UAF Department of Chemistry & Biochemistry. We would like to thank the following: A. Liljedahl, V. E. Romanovsky, R. Daanen. Further thanks to N. Ramos, D. Knight, N. Ruckhaus, R. Noratuk, A. Mutschlecner, S. Ewers, R. Davey, R. Voight, J. Spaleta, T. Harms, K. Spaleta and S. Billings for instrumentation and sampling assistance.

Author contributions KRG—conceptualization, sampling and analysis, original draft, writing, review and editing, visualization; BAE—investigation, sampling and analysis, writing, review and editing; KWA—conceptualization, investigation, review and editing; DLB—conceptualization, investigation, review and editing; JJG—conceptualization, analysis, original draft, writing, review and editing, visualization.

Funding This material is based in part upon work funded by NSF OPP-1500931, NASA through the Alaska Space Grant Program (80NSSC20M0070) Graduate Research Fellowship, and National Institutes for Water Resources Graduate Student-Led Proposal through the UAF Water & Environmental Research Center (WERC) and the USGS. Additional support to K. Walter Anthony came from NSF NNA 2022561.

Availability of data and materials The data that support the findings of this study are available from the corresponding author upon reasonable request.

Declarations

Conflict of interest The authors have no relevant financial or non-financial interests to disclose.

References

- Abbott BW, Larouche JR, Jones JB, Bowden WB, Balser A (2014) Elevated dissolved organic carbon biodegradability from thawing and collapsing permafrost. J Geophys Res: Biogeosci 119:2049–2063. https://doi.org/10.1002/2014JG002678
- Alberto M, Arah J, Neue H, Wassmann R, Lantin R, Aduna J, Bronson K (2000) A sampling technique for the determination of dissolved methane in soil solution. Chemosphere Glob Change Sci 2:57–63. https://doi.org/10.1016/S1465-9972(99)00044-6
- Bagard M-L, Chabaux F, Pokrovsky OS, Viers J, Prokuskin AS, Stille P, Rihs S, Schmitt A-D, Dupré B (2011) Seasonal variability of element fluxes in two Central Siberian rivers draining high-latitude permafrost dominated areas. Geochim Cosmochim Acta 75:3335–3357. https://doi.org/10.1016/j.gca.2011.03.024
- Barker AJ, Douglas TA, Jacobson AD, McClelland JW, Ilgen AG, Khosh MS, Lehn GO, Trainor TP (2014) Late season mobilization of trace metals in two small Alaskan arctic watersheds as a proxy for landscape scale permafrost active layer dynamics. Chem Geol 381:180–193. https://doi.org/10.1016/j.chemgeo. 2014.05.012
- Boyer A, Ning P, Killey D, Klukas M, Rowan D, Simpson AJ, Passeport E (2018) Strontium adsorption and desorption in wetlands: role of organic matter functional groups and environmental implications. Wat Res 133:27–36. https://doi.org/10.1016/j. watres.2018.01.026
- Brown EJ, Luong HV, Forshaug JM (1982) The occurrence of *Thiobacillus ferrooxidans* and arsenic in subarctic streams affected by gold-mine drainage. Arct Inst North Am 35:417–421
- Callegary JB, Kikuchi CP, Koch JC, Lilly MR, Leake SA (2013) Review: Groundwater in Alaska (USA). Hydrogeol J 21:25–39. https://doi.org/10.1007/s10040-012-0940-5
- Carey SK, Woo MK (2000) The role of soil pipes as a slope runoff mechanism, Subarctic Yukon, Canada. J Hydrol 233:206–222. https://doi.org/10.1016/S0022-1694(00)00234-1
- Chin KS, Lento J, Culp JM, Lacelle D, Kokelj SV (2016) Permafrost thaw and intense thermokarst activity decreases abundance of stream benthic macroinvertebrates. Glob Change Biol 22:2715–2728. https://doi.org/10.1111/gcb.13225
- Cory RM, Miller MP, McKnight DM, Guerard JJ, Miller PL (2010) Effect of instrument-specific response on the analysis of fulvic acid fluorescence spectra. Limnol Oceanogr Methods 8:67–78. https://doi.org/10.4319/lom.2010.8.0067
- Drake TW, Wickland KP, Spencer RGM, McKnight DM, Striegl RG (2015) Ancient low-molecular-weight organic acids in permafrost fuel rapid carbon dioxide production upon thaw. Proc Natl Acad Sci USA 112:13946–13951. https://doi.org/10.1073/pnas.1511705112
- Eckhardt BA (2020) Transport of CH4 through open-talik lakes in discontinuous permafrost aquifers. University of Alaska Fairbanks, Alaska
- Elder CD, Schweiger M, Lam B, Crook ED, Xu X, Walker J, Walter Anthony KM, Czimczik CI (2019) Seasonal sources of whole-lake CH₄ and CO₂ emissions from interior Alaskan thermokarst lakes. J Geophys Res Biogeosci 124:1209–1229. https://doi.org/10.1029/2018JG004735
- Emond AM, Daanen RP, Graham GRC, Walter Anthony KM, Liljedahl AK, Minsley BJ, Barnes DL, Romanovsky VE (2018) Airborne electromagnetic and magnetic survey, Goldstream Creek watershed, interior Alaska. Alaska Div Geol Geophys Surv Geophys Rep. https://doi.org/10.14509/29681
- US EPA (1994) Method 200.8: Determination of Trace Elements in Waters and Wastes by Inductively Coupled Plasma-Mass Spectrometry. Rev. 5.4. Cincinnati. https://www.epa.gov/esam/



- epa-method-2008-determination-trace-elements-waters-and-wastes-inductivelycoupled-plasma-mass
- Ewing SA, O'Donnell JA, Aiken GR, Butler K, Butman D, Windham-Myers L, Kanevskiy MZ (2015) Long-term anoxia and release of ancient, labile carbon upon thaw of Pleistocene permafrost. Geophys Res Lett 42:10730–10738. https://doi.org/10.1002/2015G1.066296
- Farquharson LM, Romanovsky VE, Kholodov A, Nicolsky D (2022) Sub-aerial talik formation observed across the discontinuous permafrost zone of Alaska. Nat Geosci 15:475–481. https://doi.org/ 10.1038/s41561-022-00952-z
- Frey KE, McClelland JW (2009) Impacts of permafrost degradation on arctic river biogeochemistry. Hydrol Process 23:169–182. https:// doi.org/10.1002/hyp.7196
- Frey KE, Smith LC (2005) Amplified carbon release from vast West Siberian peatlands by 2100. Geophys Res Lett 32:L09401. https://doi.org/10.1029/2004GL022025
- Gagné KR, Ewers SC, Murphy CJ, Daanen R, Walter Anthony KM, Guerard JJ (2020) Composition and photo-reactivity of organic matter from permafrost soils and surface waters in interior Alaska. Environ Sci Process Impacts 22:1525–1539. https://doi.org/10. 1039/D0EM00097C
- Grewer DM, Lafrenière MJ, Lamoureux SF, Simpson MJ (2016) Redistribution of soil organic matter by permafrost disturbance in the Canadian High Arctic. Biogeochem 128:397–415. https://doi.org/10.1007/s10533-016-0215-7
- Hansen AM, Kraus TEC, Pellerin BA, Fleck JA, Downing BD, Bergamaschi BA (2016) Optical properties of dissolved organic matter (DOM): effects of biological and photolytic degradation. Limnol Oceanogr 61:1015–1032. https://doi.org/10.1002/lno.10270
- Helms JR, Stubbins A, Ritchie JD, Minor EC, Kieber DJ, Mopper K (2008) Absorption spectral slopes and slope ratios as indicators of molecular weight, source, and photobleaching of chromophoric dissolved organic matter. Limnol Oceanogr 53:955–969. https:// doi.org/10.4319/lo.2008.53.3.0955
- Heslop JK, Winkel M, Walter Anthony KM, Spencer RGM, Podgorski DC, Zito P, Kholodov A, Zhang M, Liebner S (2019) Increasing organic carbon biolability with depth in yedoma permafrost: ramifications for future climate change. J Geophys Res: Biogeosci 124:2021–2038. https://doi.org/10.1029/2018JG004712
- Huguet A, Vacher L, Relexans S, Saubusse S, Froidefond JM, Parlanti E (2009) Properties of fluorescent dissolved organic matter in the Gironde Estuary. Org Geochem 40:706–719. https://doi.org/10.1016/j.orggeochem.2009.03.002
- Johnston SE, Bogard MJ, Rogers JA, Butman D, Striegl RG, Dorn-blaser M, Spencer RGM (2019) Constraining dissolved organic matter sources and temporal variability in a model sub-Arctic lake. Biogeochem 146:271–292. https://doi.org/10.1007/s10533-019-00619-9
- Jongejans LL, Strauss J, Lenz J, Peterse F, Mengelsdorf K, Fuchs M, Grosse G (2018) Organic matter characteristics in yedoma and thermokarst deposits on Baldwin Peninsula, west Alaska. Biogeosci 15:6033–6048. https://doi.org/10.5194/bg-15-6033-2018
- Keller K, Blum JD, Kling GW (2007) Geochemistry of soils and streams on surfaces of varying ages in arctic Alaska. Arct, Antarct, Alpine Res 39:84–98. https://doi.org/10.1657/1523-0430(2007)39[84:GOSASO]2.0.CO;2
- Kessler MA, Plug LJ, Walter Anthony KM (2012) Simulating the decadal-to millennial- scale dynamics of morphology and sequestered carbon mobilization of two thermokarst lakes in NW Alaska. J Geophys Res 117:G00M06. https://doi.org/10. 1029/2011JG001796
- Knoblauch C, Beer C, Liebner SM, Grigoriev N, Pfeiffer EM (2018) Methane production as key to the greenhouse gas budget of thawing permafrost. Nat Climate Change 8:309–312. https:// doi.org/10.1038/s41558-018-0095-z

- Kokelj SV, Lacelle D, Lantz TC, Tunnicliffe J, Malone L, Clark ID, Chin KS (2013) Thawing of massive ground ice in mega slumps drives increases in stream sediment and solute flux across a range of watershed scales. J Geophys Res Earth Surf 118:681–692. https://doi.org/10.1002/jgrf.20063
- Kurek MR, Frey KE, Guillemette F, Podgorski DC, Townsend-Small A, Arp CD, Kellerman AM, Spencer RGM (2022) Trapped under ice: Spatial and seasonal dynamics of dissolved organic matter composition in tundra lakes. J Geophys Res 127:e2021GJ006578, https://doi.org/10.1029/2021JG006578
- Lafrenière MJ, Lamoureux SF (2013) Thermal perturbation and rainfall runoff have greater impact on seasonal solute loads than physical disturbance of the active layer. Permafr Periglac Process 24:241–251. https://doi.org/10.1002/ppp.1784
- LaPerriere JD, Reynolds JB (1997) Gold placer mining and stream ecosystems of interior Alaska. In: Milner AM (ed) Freshwaters of Alaska. Springer, New York, pp 265–280. https://doi.org/10.1007/978-1-4612-0677-4_10
- Larouche JR, Abbott BW, Bowden WB, Jones JB (2015) The role of watershed characteristics, permafrost thaw, and wildfire on dissolved organic carbon biodegradability and water chemistry in Arctic headwater streams. Biogeosci 12:4221–4233. https://doi.org/10.5194/bg-12-4221-2015
- Lesh ME, Ridgway KD (2007) Geomorphic evidence of active transpressional deformation in the Tanana foreland basin, south-central Alaska. In: Ridgway KD, Trop JM, Glen JMG, O'Neill JM (eds) Tectonic growth of a collisional continental margin: crustal evolution of Southern Alaska. Geological Society of America, Boulder, pp 573–592. https://doi.org/10.1130/2007.2431(22)
- Li Y, Harir M, Uhl J, Kanawati B, Lucio M, Smirnov KS, Koch BP, Schmitt-Kopplin P, Hertkorn N (2017) How representative are dissolved organic matter (DOM) extracts? A comprehensive study of sorbent selectivity for DOM isolation. Wat Res 116:316–323. https://doi.org/10.1016/j.watres.2017.03.038
- Lockwood PV, McGarity JW, Charley JL (1995) Measurement of chemical weathering rates using natural chloride as a tracer. Geoderma 64:215–232. https://doi.org/10.1016/0016-7061(94) 00010-8
- MacDonald EN, Tank SE, Kokelj SV, Froese DG, Hutchins RHS (2021) Permafrost-derived dissolved organic matter composition varies across permafrost end-members in the western Canadian Arctic. Environ Res Lett 16:024036. https://doi.org/10.1088/1748-9326/abd971
- McNamara JP, Kane DL, Hinzman LD (1997) Hydrograph separations in an Arctic watershed using mixing model and graphical techniques. Wat Resour Res 33:1707–1719. https://doi.org/10.1029/97WR01033
- Muhs DR, Budahn JR (2006) Geochemical evidence for the origin of late Quaternary loess in central Alaska. Can J Earth Sci 43:323– 337. https://doi.org/10.1139/E05-115
- Mutschlecner AE, Guerard JJ, Jones JB, Harms TK (2018) Regional and intra-annual stability of dissolved organic matter composition and biolability in high-latitude Alaskan rivers. Limnol Oceanogr 63:1605–1621. https://doi.org/10.1002/lno.10795
- Neff JC, Finlay JC, Zimov SA, Davydov SP, Carrasco JJ, Schuur EAG, Davydova AI (2006) Seasonal changes in the age and structure of dissolved organic carbon in Siberian rivers and streams. Geophys Res Lett 33:L23401. https://doi.org/10.1029/2006GL028222
- O'Donnell JA, Jones JB (2006) Nitrogen retention in the riparian zone of catchments underlain by discontinuous permafrost. Freshw Biol 51:854–864. https://doi.org/10.1111/j.1365-2427.2006.01535.x
- O'Donnell JA, Aiken GR, Swanson DK, Panda S, Butler KD, Baltensperger AP (2016) Dissolved organic matter composition of Arctic rivers: linking permafrost and parent material to riverine



- carbon. Global Biogeochem Cycles 30:1811–1826. https://doi.org/10.1002/2016GB005482
- O'Donnell JA, Aiken GR, Kane ES, Jones JB (2010) Source water controls on the character and origin of dissolved organic matter in streams of the Yukon River basin. Alaska J Geophys Res 115:G03025. https://doi.org/10.1029/2009JG001153
- Ohno T (2002) Fluorescence inner-filtering correction for determining the humification index of dissolved organic matter. Environ Sci Technol 36:742–746. https://doi.org/10.1021/es0155276
- Ohno T, Amirbahman A, Bro R (2008) Parallel factor analysis of excitation—emission matrix fluorescence spectra of water soluble soil organic matter as basis for the determination of conditional metal binding parameters. Environ Sci Technol 42:186–192. https://doi.org/10.1021/es071855f
- Olefeldt D, Goswami S, Grosse T, Hayes D, Hugelius G, Kuhry P, McGuire AD, Romanovsky VE, Sannel ABK, Schuur EAG, Turetsky MR (2016) Circumpolar distribution and carbon storage of thermokarst landscapes. Nat Commun 7:13043. https://doi.org/10.1038/ncomms13043
- Oleinikova OV, Poitrasson F, Drozdova OY, Shirokova LS, Lapitskiy SA, Pokrovsky OS (2019) Iron isotope fractionation during bioand photodegradation of organoferric colloids in boreal humic waters. Environ Sci Technol 53:11183–11194. https://doi.org/10.1021/acs.est.9b02797
- Olid C, Rodellas V, Rocher-Ros G, Garcia-Orellana J, Deigo-Feliu M, Alorda-Kleinglass A, Bastviken D, Karlsson J (2022) Groundwater discharge as a driver of methane emissions from Arctic lakes. Nature Commun 13:3667. https://doi.org/10.1038/s41467-022-31219-1
- Petrone KC, Jones JB, Hinzman LD, Boone RD (2006) Seasonal export of carbon, nitrogen, and major solutes from Alaskan catchments with discontinuous permafrost. J Geophys Res: Biogeosci 111:G02020. https://doi.org/10.1029/2005JG000055
- Petrone KC, Hinzman LD, Shibata H, Jones JB, Boone RD (2007) The influence of fire and permafrost on sub-arctic stream chemistry during storms. Hydrol Process 21:423–434. https://doi.org/10.1002/hyp.6247
- Peuravuori J, Pihlaja K (1997) Molecular size distribution and spectroscopic properties of aquatic humic substances. Anal Chim Acta 337:133–149. https://doi.org/10.1016/S0003-2670(96)00412-6
- Pokrovsky OS, Schott J (2002) Iron colloids/organic matter associated transport of major and trace elements in small boreal rivers and their estuaries (NW Russia). Chem Geol 190:141–179. https://doi.org/10.1016/S0009-2541(02)00115-8
- Pokrovsky OS, Karlsson J, Giesler R (2018) Freeze-thaw cycles of Arctic thaw ponds remove colloidal metals and generate low-molecular-weight organic matter. Biogeochem 137:321–336. https://doi.org/10.1007/s10533-018-0421-6
- Poulin BA, Ryan JN, Aiken GR (2014) Effects of iron on optical properties of dissolved organic matter. Environ Sci Technol 48:10098–10106. https://doi.org/10.1021/es502670r
- Prokushkin AS, Gleixner G, McDowell WH, Ruehlow S, Schulze ED (2007) Source-and substrate-specific export of dissolved organic matter from permafrost-dominated forested watershed in central Siberia. Glob Biogeochem Cycles 21:GB4003. https://doi.org/10.1029/2007GB002938
- Rogers JA, Galy V, Kellerman AM, Chanton JP, Zimov N, Spencer RGM (2021) Limited presence of permafrost dissolved organic matter in the Kolyma River, Siberia revealed by ramped oxidation. JGR Biogeosci 125:32020JG005977. https://doi.org/10.1029/2020JG005977
- Schirrmeister L, Grosse G, Wetterich S, Overduin PP, Strauss J, Schuur EAG, Hubberten HW (2011) Fossil organic matter characteristics in permafrost deposits of the northeast Siberian Arctic. J Geophys Res Biogeosci 116:G00M02. https://doi.org/10.1029/2011JG001647

- Schirrmeister L, Meyer H, Andreev A, Keinast F, Bobrov A, Fuchs M, Seirralta M, Herzschuh U (2016) Late Quaternary paleoenvironmental records from the Chatanika River valley near Fairbanks (Alaska). Quat Sci Rev 147:259–278. https://doi.org/10.1016/j.guascirev.2016.02.009
- Schuur EAG, McGuire AD, Schädel C, Grosse G, Harden JW, Hayes DJ, Hugelius G, Koven CD, Kuhry P, Lawrence DM, Natali SM, Olefeldt D, Romanovsky VE, Schaefer K, Turetsky MR, Treat CC, Vonk JE (2015) Climate change and the permafrost carbon feedback, Nature 520:171–179. https://doi.org/10.1038/nature14338
- Shatilla NJ, Carey S (2019) Assessing inter-annual and seasonal patterns of DOC and DOM quality across a complex alpine watershed underlain by discontinuous permafrost in Yukon, Canada. Hydrol Earth Syst Sci 23:3571–3591. https://doi.org/10.5194/hess-23-3571-2019
- Spence CC (1994) Alaska Gold Dredging. In: Townley JM (ed) Mining history association 1994 annual. Mining History Association, Reno, pp 109–118
- Spencer RGM, Mann PJ, Dittmar T, Eglinton TI, McIntyre C, Holmes RM, Zimov N, Stubbins A (2015) Detecting the signature of permafrost thaw in Arctic rivers. Geophys Res Lett 42:2830–2835. https://doi.org/10.1002/2015GL063498
- Stolpe B, Guo L, Shiller AM (2013) Binding and transport of rare earth elements by organic and iron-rich nanocolloids in alaskan rivers, as revealed by field-flow fractionation and ICP-MS. Geochim Cosmochim Acta 106:446–462. https://doi.org/10.1016/j.gca.2012.12.033
- Stottlemyer R (2001) Biogeochemistry of a treeline watershed, northwestern Alaska. J Environ Qual 30:1990–1998. https://doi.org/10.2134/jeq2001.1990
- Strauss J, Schirrmeister L, Grosse G, Wetterich S, Ulrich M, Herzschuh U, Hubberten H-W (2013) The deep permafrost carbon pool of the Yedoma region in Siberia and Alaska. Geophys Res Lett 40:6165–6170. https://doi.org/10.1002/2013GL058088
- Strauss J, Schirrmeister L, Grosse G, Fortier D, Hugelius G, Knoblauch C, Romanovsky V, Schädel C, Schneider von Deimling T, Schuur EAG, Shmelev D, Ulrich M, Veremeeva A (2017) Deep Yedoma permafrost: a synthesis of depositional characteristics and carbon vulnerability. Earth-Sci Rev 172:75–86. https://doi.org/10.1016/j.earscirev.2017.07.007
- Strichak L, Donaldson DJ (2021) Relating natural organic matter conformation, metal complexation, and photophysics. Can J Chem 99:787–794. https://doi.org/10.1139/cjc-2021-0018
- Striegl RG, Aiken GR, Dornblaser MM, Raymond PAW, KP, (2005) A decrease in discharge-normalized DOC export by the Yukon River during summer through autumn. Geophys Res Lett 32:L21413. https://doi.org/10.1029/2005GL024413
- Striegl RG, Dornblaser MM, Aiken GR, Wickland KP, Raymond PA (2007) Carbon export and cycling by the Yukon, Tanana, and Porcupine rivers, Alaska. 2001–2005. Wat Resour Res 43:W02411. https://doi.org/10.1029/2006WR005201
- Thienpont JR, Rühland KM, Pisaric MFJ, Kokelj SV, Kimpe LE, Blais JM, Smol JP (2013) Biological responses to permafrost thaw slumping in Canadian Arctic lakes. Freshw Biol 58:337–353. https://doi.org/10.1111/fwb.12061
- Toohey RC, Herman-Mercer NM, Schuster PF, Mutter EA, Koch JC (2016) Multidecadal increases in the Yukon River Basin of chemical fluxes as indicators of changing flowpaths, groundwater, and permafrost. Geophys Res Lett 43:12120–12130. https://doi.org/ 10.1002/2016GL070817
- Vonk JE, Mann PJ, Dowdy KL, Davydova A, Davydov SP, Zimov N, Spencer RGM, Bulygina EB, Eglinton TI, Holmes RM (2013) Dissolved organic carbon loss from Yedoma permafrost amplified by ice wedge thaw. Environ Res Lett 8:035023. https://doi.org/10. 1088/1748-9326/8/3/035023



- Vonk JE, Tank SE, Bowden WB, Laurion I, Vincent WF, Alekseychik P, Amyot M, Billet MF, Canário J, Cory RM, Deshpande BN, Helbig M, Jammet M, Karlsson J, Larouche J, MacMillan G, Rautio M, Walter Anthony KM, Wickland KP (2015) Reviews and syntheses: effects of permafrost thaw on Arctic aquatic ecosystems. Biogeosci 12:7129–7167. https://doi.org/10.5194/bg-12-7129-2015
- Walter Anthony KM, Zimov SA, Grosse G, Jones MC, Anthony PM, Chapin FS III, Finlay JC, Mac MC, Davydov S, Frenzel P, Frolking S (2014) A shift of thermokarst lakes from carbon sources to sinks during the Holocene epoch. Nature 511:452–456. https://doi.org/10.1038/nature13560
- Walter Anthony K, Schneider von Deimling T, Nitze I, Frolkin S, Emond A, Daanen R, Anthony P, Lindgren P, Jones B, Grosse G (2018) 21St-century modeled permafrost carbon emissions accelerated by abrupt thaw beneath lakes. Nat Commun 9:3262. https:// doi.org/10.1038/s41467-018-05738-9
- Walter Anthony KM, Lindgren P, Hanke P, Engram M, Anthony P, Daanen RP, Bondurant A, Liljedahl AK, Lenz J, Grosse G, Jones BM, Brosius L, James SR, Minsley BJ, Pastick NJ, Munk J, Chanton JP, Miller CE, Meyer FJ (2021) Decadal-scale hotspot methane ebullition within lakes following abrupt permafrost thaw. Environ Res Lett 16:035010. https://doi.org/10.1088/1748-9326/abc848

- Weishaar JL, Aiken GR, Bergamaschi BA, Fram MS, Fujii R, Mopper K (2003) Evaluation of specific ultraviolet absorbance as an indicator of the chemical composition and reactivity of dissolved organic carbon. Environ Sci Technol 37:4702–4708. https://doi.org/10.1021/es030360x
- Weyhenmeyer GA, Prairie YT, Tranvik LJ (2014) Browning of boreal freshwaters coupled to carbon-iron interactions along the aquatic continuum. PLoS ONE 9:e88104
- Winkel M, Sepulveda-Jauregui A, Martinez-Cruz K, Heslop JK, Rijkers R, Horn F, Liebner S, Walter Anthony KM (2019) First evidence for cold- adapted anaerobic oxidation of methane in deep sediments of thermokarst lakes. Environ Res Commun 1:021002. https://doi.org/10.1088/2515-7620/ab1042
- Yoshikawa K, Hinzman LD (2003) Shrinking thermokarst ponds and groundwater dynamics in discontinuous permafrost near Council, Alaska. Permafr Periglac Process 14:151–160. https://doi.org/10.1002/ppp.451

Publisher's Note Springer Nature remains neutral with regard to jurisdictional claims in published maps and institutional affiliations.

